Approaches for Co-Sintering Metal-Supported Proton-Conducting Solid Oxide Cells with $Ba(Zr,Ce,Y,Yb)O_{3-\delta}$ Electrolyte

Ruofan Wang[1], Grace Y. Lau[1], Dong Ding[2], Tianli Zhu[3], and Michael C. Tucker[1*]

1. Energy Conversion Group, Energy Storage and Distributed Resources Division, Lawrence Berkeley National Laboratory, Berkeley, California, United States

2. Energy & Environmental Science and Technology, Idaho National Laboratory, Idaho Falls, ID

3. United Technologies Research Center, East Hartford, CT

Corresponding author: Michael C. Tucker, mctucker@lbl.gov, Tel +1 (510) 486-5304, 1 Cyclotron Road, MS 62-203, Berkeley, CA 94720, United States

Abstract

Proton conducting oxide electrolyte materials could potentially lower the operating temperature of metal-supported solid oxide cells (MS-SOCs) to the intermediate range 400 to 600 °C. The porous metal substrate provides the advantages of MS-SOCs such as high thermal and redox cycling tolerance, low-cost of structural materials, and mechanical ruggedness. In this work, the viability of co-sintering fabrication of metal-supported proton conducting solid oxide cells using $BaZr_{1-x-y}Ce_xY_yO_{3-\delta}$ (BZCY) is investigated. BZCY ceramics are sintered at 1450 °C in reducing environment alone and supported on Fe-Cr alloy metal support, and key characteristics such as Ba loss, sintering behavior, and chemical compatibility with metal support are determined. Critical challenges are identified for this fabrication approach, including: contamination of the electrolyte with Si and Cr from the

metal support, incomplete electrolyte sintering, and evaporation of electrolyte constituents. Various approaches to overcome these limitations are proposed, and preliminary assessment indicates that the use of barrier layers, low-Si-content stainless steel, and sintering aids warrant further development.

Keywords: Protonic ceramic electrolysis cells; Protonic ceramic fuel cells; Metal supported; Protonic ceramic electrochemical cells; Doped barium zirconate; BZCY

1. Introduction

Proton-conducting oxide ceramics are widely explored as alternatives to conventional oxide conductors, primarily because the proton conductors display higher conductivity at intermediate temperatures (400-600 °C). Use of proton conducting electrolytes in solid oxide fuel cells (SOFCs) and electrolysis cells (SOECs) enables efficient operation at lower temperatures, reducing thermal stress and allowing the use of less expensive stack materials and balance-of-plant components. Figure 1 illustrates metal-supported protonic ceramic cells operating in fuel cell and electrolysis conditions. Transport of protons across the electrolyte offers other advantages at all temperatures: for electrolysis, pure hydrogen is produced so steam does not need to be removed from the product stream; for fuel cell operation, extraction of hydrogen from the anode through the electrolyte can drive fuel decomposition or reforming reactions forward. Protonic ceramic fuel cells (PCFCs) furthermore resist carbon coking and are tolerant to sulfur, enabling stable operation with a wide variety of hydrocarbon fuels [1,2]. Operation with nitrogen-based fuels such as ammonia and hydrazine has also been demonstrated [3]. Barium cerium zirconate doped with yttria (BZCY) or other

dopants is the most widely used proton conductor for solid oxide cells (SOCs), due to its high conductivity [4–6]. There is a tradeoff between stability in the presence of carbon dioxide vs. high conductivity, sinterability and grain growth, with the Ce:Zr ratio being a key controlling factor [5]. Doping with Y and Yb yields improvement in conductivity [5]. In this work, we utilize a standard commercially-available composition BZCY721 (Ba $Zr_{0.7}Ce_{0.2}Y_{0.1}O_{3-\delta}$) [7], as well as compositions with higher Ce content and addition of Yb, BZCYYb4411 ($BaZr_{0.4}Ce_{0.4}Y_{0.1}Yb_{0.1}O_{3-\delta}$) and BZCYYb1711 ($BaZr_{0.1}Ce_{0.7}Y_{0.1}Yb_{0.1}O_{3-\delta}$) [2,8].

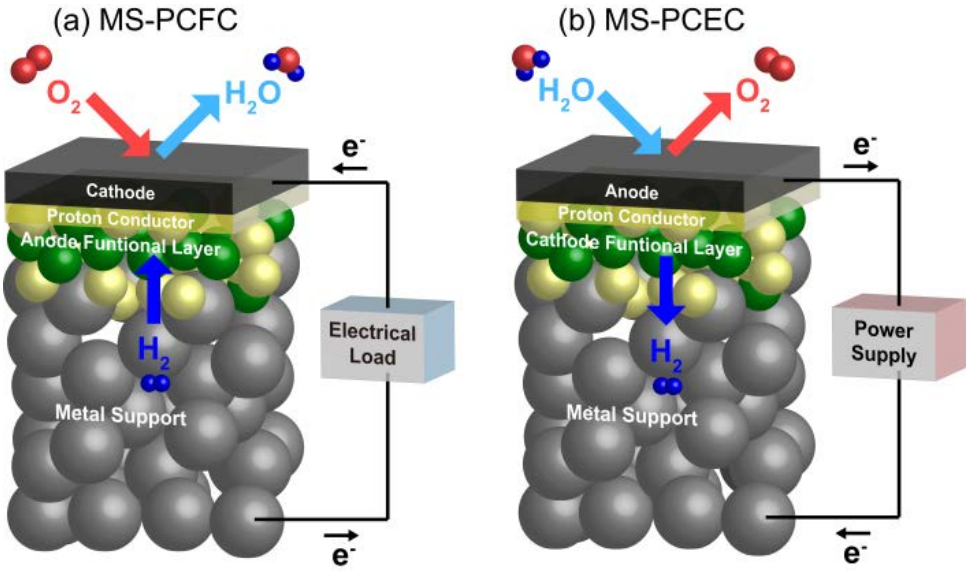

Figure 1. Cell architecture. Schematic representation of (a) metal supported protonic ceramic fuel cell (MS-PCFC), and (b) metal supported protonic ceramic electrolysis cell (MS-PCEC). Only a thin portion of the hydrogen electrode layer, as required for electrochemical function, is retained in the MSC design. (Reproduced with permission from Ref. [9]).

Metal-supported solid oxide cells (MS-SOCs) incorporate thin layers of electrochemically-active ceramics supported on thicker metal layers that provide mechanical support and electronic current collection. MS-SOFCs promise high performance provided by the active ceramic layers, and excellent mechanical properties and low materials cost derived from the metal support. Ferritic stainless steel is a typical choice for the metal support, as it displays good oxidation resistance below about 800 °C, has a coefficient of thermal expansion that is similar to common SOFC ceramic materials, and is very inexpensive compared to other alloys with similar corrosion resistance. In contrast to conventional all-ceramic SOCs, MS-SOCs offer further operational advantages including: mechanical ruggedness; tolerance to very rapid thermal cycling both during start-up and variable operation [10–12]; and tolerance to oxidation of the fuel catalyst, which occurs during high fuel utilization, intermittent fuel use, or unexpected loss of fuel supply (i.e. due to failure in the fuel delivery subsystem) [13,14]. Because of these cost and operational advantages, MS-SOCs are being developed for applications that require fast-start or intermittent operation, including personal power generators [12,15], residential combined heat and power [14], vehicle range extenders [16–18], and electrolysis cells for conversion of variable power sources such as wind and solar [19–21]. Details of MS-SOC materials selection, cell architecture, processing approaches, and notable cell and system demonstrations are available in various review articles [22–24].

Given the advantages of PCFCs and MS-SOCs discussed above, it is of interest to develop metal-supported protonic ceramic electrochemical cells with BZCY-based electrolyte. Recently, Stange et al. successfully prepared a complete half-cell on ferritic stainless steel support, with barium yttrium zirconate-Ni (BZY-Ni) electrode and BZY electrolyte deposited

by pulsed laser deposition (PLD) [25,26]. Under electrolysis conditions (hydrogen vs. steam), the cell displayed a high total resistance of 40 Ohm·cm^2 at 600 °C, indicating that significant optimization effort remains to achieve the performance expected for a BZY-based cell. Reactive spray deposition technology (RSDT) has also been used to successfully apply multiple ceramic cell layers including dense BYZ electrolyte on pre-sintered ferritic stainless steel support, but cell performance is not reported [27,28].

Compared to PLD and RSDT, co-sintering is an attractive option for fabricating MS-SOCs due to the conventional low-cost, high-throughput manufacturing techniques used to deposit the ceramic layers (e.g. tape-casting, screen-printing, aerosol spray deposition), and the relatively high processing temperature resulting in a dense electrolyte layer with high conductivity [22]. The limited work on co-sintering BZCY with stainless steel support indicates, however, that significant challenges exist for this approach. Mercadelli et al. co-sintered BZCY-Ni anodes supported on ferritic stainless steel, finding that interdiffusion between the anode and steel layers was a significant issue and resulted in contamination of the Ni catalyst and melting of the stainless steel [29]. Although the authors were successful in minimizing interdiffusion via addition of a ceria barrier layer, a complete cell was not fabricated. Our recent effort to screen a wide variety of proton conducting ceramics for compatibility with co-sintering on ferritic stainless steel revealed that BZCY survives sintering in reducing atmosphere (required to avoid oxidation of the stainless steel), but reacts deleteriously with the metal support [9]. In particular, a large amount of Si and minor amount of Cr from the stainless steel migrated into the BZCY layers. After sintering, the electrolyte layer was composed of a mixture of BZCY and a significant amount of Ba_2SiO_4.

Furthermore, BZCY achieved only 73% of theoretical density and experienced significant Ba evaporation after sintering at 1450°C in reducing atmosphere.

Here, we explore these challenges in more detail and propose several approaches to overcome them. The impact of Ce:Zr ratio in BZCY, sintering temperature, stainless steel composition, and addition of a Si-diffusion barrier layer are explored. Based on preliminary results, promising directions for future development of metal-supported BZCY cells are discussed.

2. Experimental section

2.1 Materials

Complete symmetric MS-SOFCs with yttria-stabilized zirconia (YSZ, Tosoh) ceramic layers were prepared by tapecasting, debinding in air, and sintering in reducing atmosphere (2% hydrogen in argon) as described elsewhere [16,21,30]. Catalysts were not added. These cells were sintered at various temperatures to investigate the impact of sintering temperature on the metal support structure, in order to select an appropriate maximum sintering temperature for cells with BZCY electrolyte.

BZCY721 ($BaZr_{0.7}Ce_{0.2}Y_{0.1}O_{3-\delta}$) powder was purchased from CerpoTech, Norway, BZCYYb4411 ($BaZr_{0.4}Ce_{0.4}Y_{0.1}Yb_{0.1}O_{3-\delta}$) powder was provided by United Technologies Research Center, BZCYYb1711 ($BaZr_{0.1}Ce_{0.7}Y_{0.1}Yb_{0.1}O_{3-\delta}$) powder was provided by Idaho National Laboratory, and CGO (10 mol% gadolinium-doped ceria) powder was provided by DKKK, Japan. Commercial powders were used as sintering aids: Co_3O_4, ZnO, NiO (all

<50nm, Sigma-Aldrich) and LiF (<10 μm, Sigma-Aldrich). Sintering aid powders were used as-received, with the exception of LiF, which was attritor milled with isopropyl alcohol for 1 h to reduce particle size before use. Commercially available ferritic stainless steel P434L alloy (water atomized, Ametek Specialty Metal Products) was used as the standard metal support material for all experiments unless otherwise noted. A low-Si 70Fe30Cr (Ametek) was used as an alternative, Table 1.

	Fe	Cr	Mo	Si	Mn	P	C	S	O
P434L	Bal	16.66	0.94	0.85	0.14	0.016	0.012	0.006	-
70Fe30Cr	Bal	29.41	-	0.46	0.16	0.01 max	0.022	0.011	0.99

Table 1. Composition of metal support alloys (wt%).

2.2 Dilatometry and sintering properties

Ceramic powders were ball-milled in isopropyl alcohol with fish oil and polyvinyl butyral as binders, dried, sieved to <150 μm, and pressed into pellets (diameter of ~6.35 mm, thickness of ~2 mm). Sintering aids were added at 2 wt% loading during ball milling. Sintering behavior of the pellets was examined using a vertical dilatometer (Linseis L75). Uniaxial shrinkage of the pellets was measured as a function of temperature up to 1450 °C, in both dry air or 2% H_2-Ar (reducing) environments, both gases used straight from the cylinder without additional drying.

Pellets and thin films of ceramic were also sintered in air (muffle furnace) or reducing environment (tube furnace with 2% H_2-Ar flow at 100 mL min^{-1}), without any compression. Thin films were prepared by brush-painting a mixture of ceramic powder and acrylic binder (Liquitex) onto a dense YSZ substrate (Fuel Cell Materials). The shrinkage, weight loss via

evaporation, and sintered density of the pellets were obtained by measuring the dimensions and weight before and after sintering. Sintered ceramics were examined by scanning electron microscopy (SEM, Hitachi TM-1000 or JEOL JSM-7500F) and energy X-ray dispersive spectroscopy (EDS, Thermo Scientific) to evaluate their grain size, porosity, and composition change. Si and Cr contents were averaged over the entire thickness of the ceramic layer, except where noted.

2.3 Metal-supported cell fabrication

Complete metal-supported half-cells were fabricated with BZCY electrolyte and electrode backbone. A green metal support sheet was tape casted and cut into 30mm diameter circles using a laser cutter (Hobby model, Full Spectrum Laser). The circular supports were fired in a box furnace at 525 °C for 1 h to remove the binder and pore former and bisque fired in a tube furnace at 1050 °C for 2 h with 2% H_2-Ar flowing (reducing environment) to provide mechanical integrity for further ceramic deposition. Three layers of ceramic powders were applied sequentially, including (a) a BZCY hand-painted porous bridging and barrier layer for bridging the pores on the metal support surface, providing a smoother surface for subsequent layers (b) a BZCY hand-painted porous electrode layer with fine pores for catalyst infiltration and obtaining a smooth surface for electrolyte deposition, and (c) an aerosol sprayed BZCY electrolyte layer. For the case of barrier layers (Section 3.3), the first layer was replaced with bridging and porous electrode layers containing CGO instead of BZCY. Details of deposition procedures of electrode and electrolyte layers are provided in Supplementary Note 1. After the deposition of the ceramic layers, cells were fired in air at 525 °C for 1 h to remove acrylic, pore formers, and residual solvent. Cells were then sintered

for 4 h in 2% H_2-Ar environment at 1450°C with gas used straight from the cylinder without additional drying, unless indicated otherwise.

3. Results and Discussion

Sintering BZCY below 1500°C is challenging, and the requirement of using reducing atmosphere for co-sintering with metal support complicates selection of a viable approach. Of particular concern is Si migration into BZCY from the metal support, and achieving densification of the BZCY electrolyte layer. Here, we explore whether increasing the Ce:Zr content is a viable approach to promote sintering in reducing atmosphere, determine the impact of sintering temperature on Si migration, assess the use of a low-Si-content metal support, and introduce a barrier layer to minimize Si transport.

3.1 Sintering behavior

3.1.1 Metal support

MS-SOFCs with YSZ electrolyte are typically sintered in the temperature range of 1250 to 1400°C [20,30–32]. Higher sintering temperature is expected to be required for full densification of BZCY ceramics. Over-densification of the metal is a concern when sintering at higher temperature, especially above 1450°C as clearly seen in cross-section images of MS-SOFCs with YSZ ceramic layers sintered at various temperatures, Figure 2. This is not surprising, as the stainless steel melting point is around 1525°C. To be compatible with co-sintering on metal support, the ceramic layer will ideally densify completely at 1450 °C or below, with shrinkage somewhat less than the bare metal (~20%) [30]. This upper sintering temperature limit is used throughout the rest of this work.

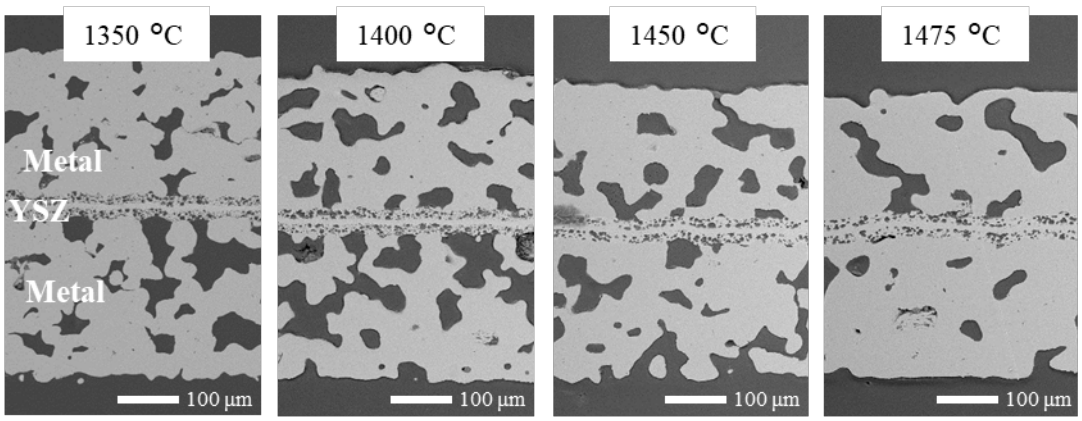

Figure 2. Metal densification. SEM cross-section images of symmetric MS-SOC structure with YSZ ceramic layers after sintering for 2 h at 1350, 1400, 1450, and 1475 °C.

3.1.2 BZCY

To elucidate sintering behavior of BZCY in the absence of metal support, dilatometry and pellet densification was conducted in air and reducing atmosphere. Sintering starts around 900 °C and continues gradually to 1450 °C, Figure 3. A plateau indicating completion of sintering is not observed, although sintering continues throughout the hold at 1450°C. This is consistent with the residual porosity and incomplete densification seen for furnace-sintered pellets, Figures 3 and Table 2. Sintering of the compositions containing Yb and with higher Ce content is delayed relative to BCZY271, but their sintering curves are steeper above about 1250°C resulting in significantly better densification at 1450°C. This appears to be related to the Ce and Yb composition, as particle size of all powders was similar. The sintering atmosphere does not have a large impact on the timing of sintering, nor the final density achieved. The enhanced sintering for higher Ce and Yb content seen here for both atmospheres is consistent with the results from sintering in air [33]. The pellets sintered in

reducing atmosphere shrank 17-18%, which is compatible with the metal support shrinkage [30].

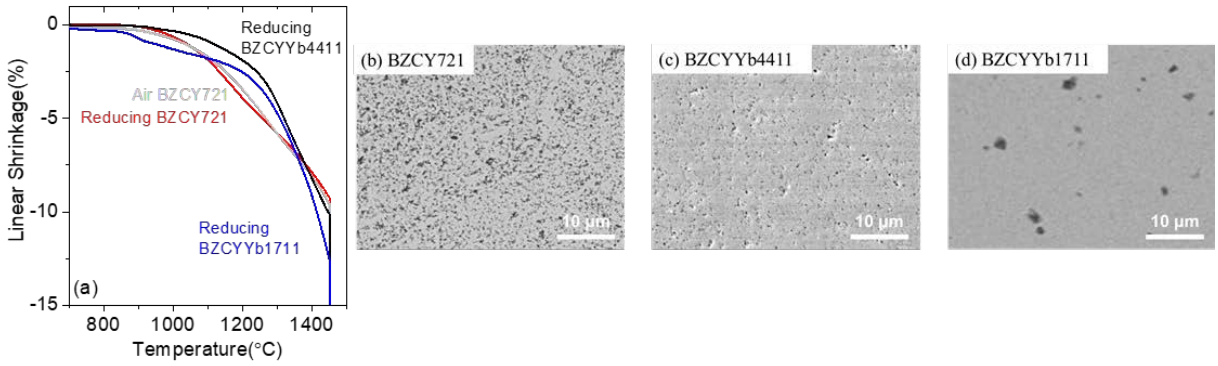

Figure 3. Sintering behavior of BZCY721, BZCYYb4411, and BZCYYb1711. (a) dilatometry and (b-d) cross-section SEM images of pellets sintered in a reducing tube furnace at 1450°C in 2% H_2/Ar for 4 h.

Composition	Sintering environment	Sintered density (g/cm^3)	Density (% of theor.)
BZCY721	Air	4.6	74
	Reducing	4.5	73
BZCYYb4411	Air	5.7	92
	Reducing	5.8	94
BZCYYb1711	Air	5.9	95
	Reducing	6.1	98

Table 2. Densification of BZCY721, BZCYYb4411, and BZCYYb1711. Density of pellets after sintering in air or reducing atmosphere (2% H_2-Ar) at 1450 °C for 2 h. Theoretical densities are provided in Refs [7,34].

Ba loss via evaporation is known to occur during sintering in air, and is detrimental to proton conductivity [35,36]. Here, the impact of reducing atmosphere and temperature are assessed. Thin layers of ceramic powder were painted onto YSZ substrates, and sintered at 1450 °C in

reducing atmosphere. Evaporative loss of Ba was determined with EDS, Figure 4. Ba loss increases with increasing sintering temperature, and is exacerbated by sintering in reducing atmosphere at 1400 °C and above, presenting an additional challenge for co-sintering with metal support. The reason for the atmosphere-dependence of the Ba evaporation rate is not clear at this point. The sample architecture was intended to be a worst-case scenario in which the thin electrolyte layer is the only source of Ba. Ba loss would presumably be mitigated by adding a Ba source to the electrolyte [35], or by the presence of other Ba-containing cell layers, an external bed of Ba-containing powder surrounding the cell [37], or Ba-saturated processing atmosphere.

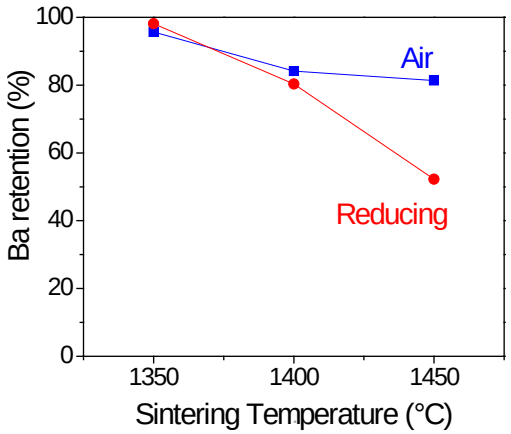

Figure 4. Impact of temperature and sintering atmosphere on Ba loss. Ba content of ~ 10μm BZCYYb4411 electrolyte film after sintering at various temperatures in air (blue squares) or reducing atmosphere (red circles), normalized to as-received powder.

3.2 Si and Cr migration

Significant migration of Ba, Zr, Ce, Y, or Yb into the metal upon co-sintering was not observed, Figure S2. In contrast, our previous work demonstrated that Si and Cr migration from the stainless steel to the BZCY electrolyte does occur during co-sintering, leading to formation of Ba_2SiO_4 and $BaCrO_4$, and depletion of Ba from the proton conducting phase [9]. This is expected to be detrimental to electrolyte performance, as the conductivity of BZCY is known to be highly sensitive to Ba content [35,38], reaction with Cr is known to be detrimental [39,40], and Ba_2SiO_4 and $BaCrO_4$ are inactive and would block the proton transport pathway. Here, the extent of migration is determined for a range of BZCY and stainless steel compositions and over a range of co-sintering temperatures, Figure 5.

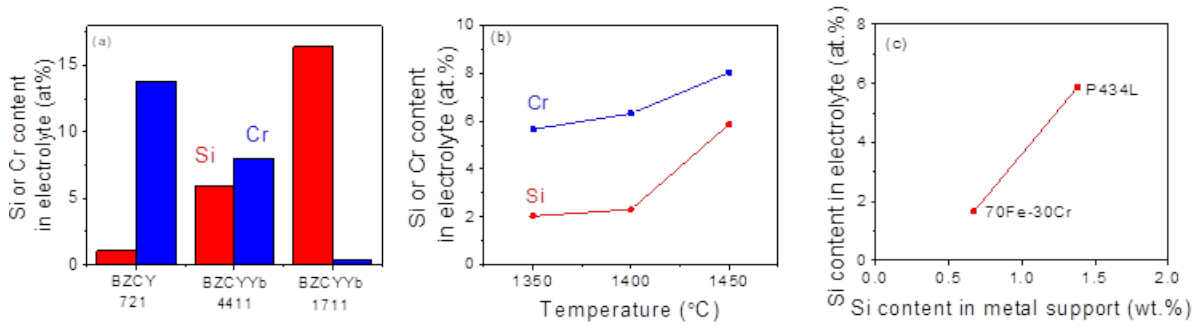

Figure 5. Si and Cr migration from the stainless steel support to the electrolyte layer during co-sintering. Impact of (a) electrolyte composition, (b) sintering temperature, and (c) Si content in the metal support, as determined by EDS analysis. The support was 434 stainless steel, the electrolyte was BZCYYb4411, and sintering temperature was 1450°C, except as noted.

Si migration increases and Cr migration decreases dramatically with increasing Ce and Yb content, Figure 5a. Si, and to a lesser extent Cr, migration can be curtailed by lowering the sintering temperature below 1450°C, Figure 5b, due to reduced Si vapor pressure and Cr

diffusivity, and also reduced reactivity between Si/Cr and BZCY at lower temperature. It is expected that Si evaporates from the metal and migrates via vapor diffusion, presumably creating a Si-saturated atmosphere throughout the vicinity of the cell. In contrast, Cr is expected to migrate via solid state diffusion, consistent with the linear gradient in Cr concentration from the metal support to the exposed side of the electrolyte, Figure S1. Reducing the sintering temperature appears to be a promising approach, if densification can be achieved at lower temperature. The use of sintering aids to achieve this goal is discussed below in Section 3.4.

Commercial ferritic stainless steels generally contain some Si, which is added as a deoxidizing agent during steel melting and to improve oxidation resistance of the steel product. Si content does vary between batches and grades of stainless steel, and presumably could be minimized intentionally when optimizing a stainless steel composition for use in a metal-supported BZCY cell. To assess if minimizing the Si content in the metal support is a useful approach, we determined Si migration from two commercial stainless steel supports with differing Si content, Figure 5c. Indeed, the extent of Si migration is quite sensitive to the Si content in the stainless steel. While promising, this approach likely requires the assistance of a stainless steel vendor and may increase the material cost due to low production volume compared to standard compositions.

To summarize, we believe that lowering the sintering temperature and Si content of the stainless steel are both viable approaches to minimizing migration. Determining the impact of various Si and Cr contents in the electrolyte layer on conductivity, thermal expansion,

mechanical properties and other metrics upper is recommended as future work. This would establish acceptable limits of Si and Cr content in the electrolyte layer to guide further efforts to suppress migration.

3.3 Barrier layer

Barrier layers have been used to block undesired migration of elements between adjacent layers in a variety of SOFC architectures [22,29,41]. Here, we find that this is an effective approach for reducing Si and Cr migration from the stainless steel support to the ceramic layers. Our initial trial uses CGO as the barrier layer, chosen because it was previously reported that BZCY and CGO do not significantly interdiffuse or react with each other when sintering in reducing atmosphere at 1400°C [42]. Si and Cr content are reduced to 2 and 0.3 at%, respectively, upon introduction of the barrier layer, Figure 6. This is a substantial improvement over the 5.9 and 8 at% contamination for Si and Cr observed for the same BZCYYb composition and sintering conditions (Figure 5a, BZCYYb4411). While the positive impact of the barrier layer on Si and Cr migration is clear, more work remains to understand the mechanism and facilitate this approach. The BZCYYb electrolyte layer must be further densified, Figure 6b, possibly by addition of a sintering aid. Also, many cracks were observed in the ceramic layers, Figure 6a, suggesting that drying, debinding, or co-sintering stresses, and shrinkage match between the layers must be improved to achieve uniform, defect-free ceramic layers.

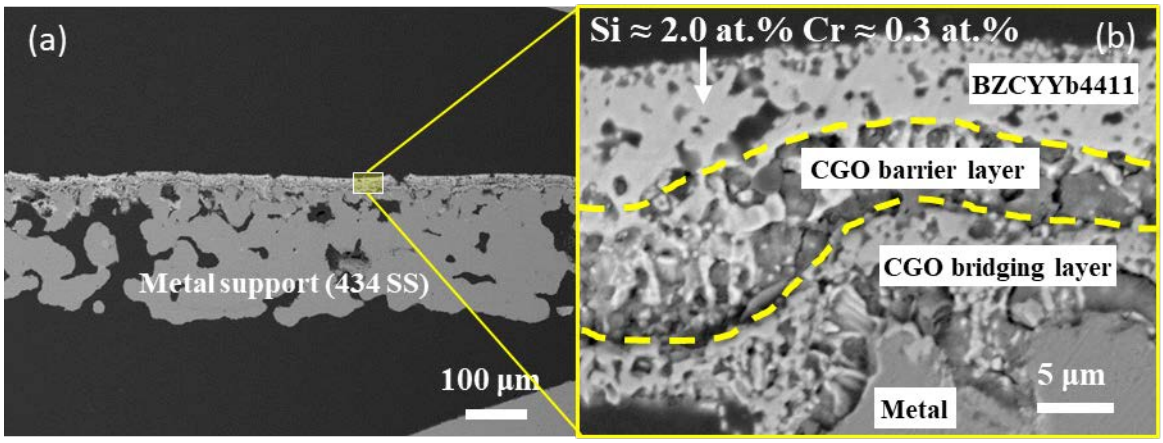

Figure 6. Impact of barrier layer on Si migration. SEM images of polished cross section microstructure of BZCYYb441 electrolyte layer co-sintered on 434 stainless steel support, with CGO layers between the support and electrolyte.

3.4 Sintering aids

Lowering the sintering temperature is desirable for several reasons including: 1) minimizing Si and Cr migration (Section 3.2); 2) preventing over-densification of the metal support (Section 3.1.1); 3) reducing Ba evaporation (Section 3.1.2); and 4)reducing processing cost. As discussed above in Sections 3.1 and 3.2, increasing Ce and Yb content enhances sintering, but also dramatically increases contamination of the electrolyte layer with Si. The use of sintering aids is another approach to reduce sintering temperature that is widely used for BZCY processing in air [43–46]. We are not aware of any reports on the effectiveness of sintering aids in reducing atmosphere.

The effectiveness of various sintering aids (Co-, Zn-, and Ni-oxides and LiF, all 2 wt%) is compared for air and reducing atmospheres in Figure 7 and Table 3. All sintering aids

significantly enhanced densification in air. The oxide sintering aids were much less effective in reducing atmosphere, however, providing final density less than 90% and microstructure with pervasive porosity. This is not surprising, as these oxides are expected to be reduced to metals in reducing atmosphere, and likely segregate from the ceramic BZCY phase. The sintering temperature is also well above the boiling point of Zn, and close to the melting points of Co and Ni, so evaporative loss of the sintering aid is also a concern. In contrast, LiF is a very effective sintering aid in reducing atmosphere, providing final density of 94% and dense microstructure with minimal open porosity. Dilatometry in reducing atmosphere reveals that incipient sintering occurs 300°C lower and sintering proceeds more rapidly with LiF addition, Figure 7b. This is similar to the sintering enhancement in air observed by Tsai et al. for a range of BZCY compositions with significantly higher LiF addition (7wt%) [44]. They showed that LiF enhances sintering in air through a liquid phase mechanism, after which all of the Li and most of the F evaporates, and that the conductivity and mechanical properties were improved by LiF addition. Presumably, a liquid phase mechanism for sintering enhancement is also predominant in reducing atmosphere.

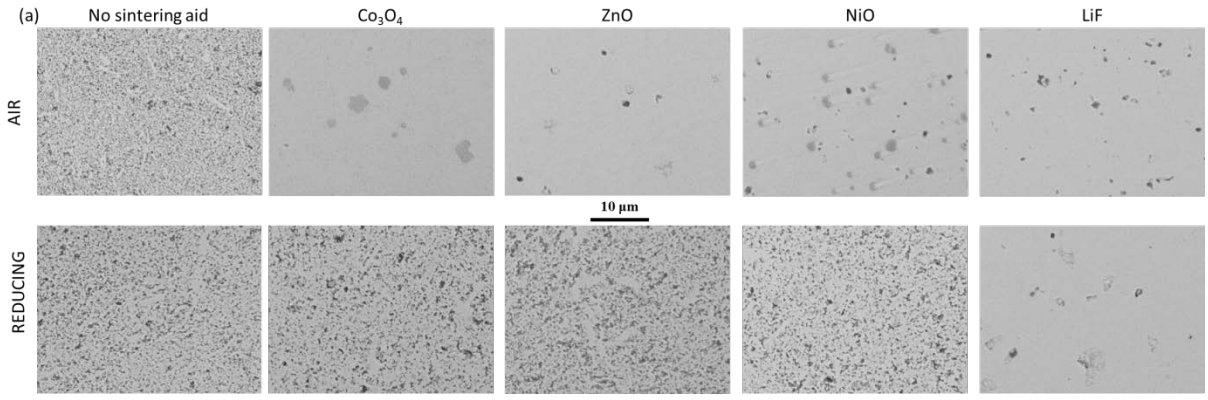

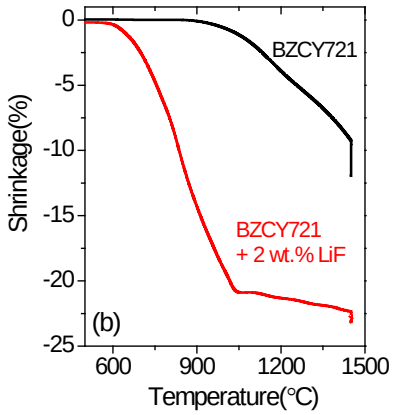

Figure 7. Impact of sintering aids. (a) SEM images of polished cross section microstructure of BZCY721 sintered with various sintering aids (2 wt%) in air (top row) and reducing atmosphere (bottom row) at 1450°C. (b) Dilatometry of BZCY721 with (red) and without (black) 2 wt% LiF in reducing atmosphere.

We prepared metal-supported electrode (porous) and electrolyte (dense) layers of BZCYYb4411 with 2 wt.% LiF by co-sintering at the reduced temperature of 1300°C, Figure 8. The electrolyte is visibly densified, and contained no detectable Cr and only 0.4 at% Si (compared to 5.8 at% for BZCYYb4411 at 1450°C, Figure 5a) as a result of the lower sintering temperature. The ceramic layer sintering was so enhanced by LiF addition that the shrinkage was no longer matched well to the metal support, leading to cracking and curvature of the ceramic layers. Improving metal shrinkage at 1300°C and below will be a subject of future effort. The impact of LiF addition on conductivity, mechanical properties, and other metrics should be assessed in the future. Effort to discover other sintering aids that are effective in reducing atmosphere may also be fruitful.

Sintering atmosphere	Sintering aid	Sintered density (g/cm^3)	Density (% of theor.)
Air	None	4.6	74
	Co_3O_4	6.0	97
	ZnO	6.0	97
	NiO	6.1	99
	LiF	5.6	91
Reducing	None	4.5	73
	Co_3O_4	5.2	84
	ZnO	4.8	77
	NiO	5.5	89
	LiF	5.8	94

Table 3. Impact of sintering aids on densification of BZCY721. Density of pellets after sintering in air or reducing atmosphere (2% H_2-Ar) at 1450 °C for 2 h. Sintering aid loading is 2 wt%. Theoretical densities are provided in Refs [7,34].

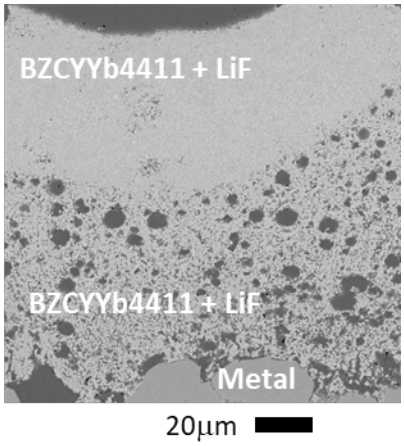

Figure 8. Reduced sintering temperature. SEM images of polished cross section microstructure of electrolyte and porous electrode layers composed of BZCYYb4411 with LiF sintering aid (2 wt%) co-sintered on metal support at 1300°C.

4. Conclusions

In this work, the viability of co-sintering fabrication of metal-supported proton conducting solid oxide cells using $BaZr_{1-x-y}Ce_xY_yO_{3-\delta}$ (BZCY) was investigated. Critical challenges were identified for this fabrication approach, including: contamination of the electrolyte with Si and Cr from the metal support, incomplete electrolyte sintering, and evaporation of Ba. Reducing the sintering temperature mitigates Ba loss and Si/Cr migration. LiF was found to be an effective sintering aid to enable this approach. Insertion of a diffusion barrier layer and the use of low-Si-content stainless steel were found to be effective in reducing Si migration. We anticipate that the results of this work will guide further efforts to fabricate a functional metal-supported BZCY-electrolyte cell via co-sintering. In particular, the use of barrier layers, low-Si-content stainless steel, and sintering aids warrants further development.

ACKNOWLEDGEMENTS

The authors gratefully acknowledge Conor Byrne for technical support on preliminary work that inspired this effort, and John Yamanis (ElectroChem Ventures LLC) for helpful discussion. This work is supported by the U.S. Department of Energy (USDOE), Office of Energy Efficiency and Renewable Energy (EERE), Fuel Cell Technologies Office (FCTO) under contract no. DE-EE0008080. This work was funded in part by the U.S. Department of Energy under contract no. DE-AC02-05CH11231.

DISCLAIMER

expressed or implied, or assumes any legal liability or responsibility for the accuracy, completeness, or usefulness of any information, apparatus, product, or process disclosed, or represents that its use would not infringe privately owned rights.

References

[1] Duan C, Kee RJ, Zhu H, Karakaya C, Chen Y, Ricote S, et al. Highly durable, coking and sulfur tolerant, fuel-flexible protonic ceramic fuel cells. Nature 2018;557:217–22. doi:10.1038/s41586-018-0082-6.

[2] Yang L, Wang S, Blinn K, Liu M, Liu Z, Cheng Z, et al. Enhanced Sulfur and Coking. Science (80-) 2009;326:126–9.

[3] Lin Y, Ran R, Guo Y, Zhou W, Cai R, Wang J, et al. Proton-conducting fuel cells operating on hydrogen, ammonia and hydrazine at intermediate temperatures. Int J Hydrogen Energy 2010;35:2637–42. doi:10.1016/j.ijhydene.2009.04.019.

[4] Bi L, Boulfrad S, Traversa E. Steam electrolysis by solid oxide electrolysis cells (SOECs) with proton-conducting oxides. Chem Soc Rev 2014;43:8255–70. doi:10.1039/c4cs00194j.

[5] Fabbri E, Pergolesi D, Traversa E. Materials challenges toward proton-conducting oxide fuel cells: A critical review. Chem Soc Rev 2010;39:4355–69. doi:10.1039/b902343g.

[6] Lefebvre-Joud F, Gauthier G, Mougin J. Current status of proton-conducting solid oxide fuel cells development. J Appl Electrochem 2009;39:535–43. doi:10.1007/s10800-008-9744-7.

[7] Cerpotech. No Title n.d.

[8] Choi S, Kucharczyk CJ, Liang Y, Zhang X, Takeuchi I, Ji H Il, et al. Exceptional power density and stability at intermediate temperatures in protonic ceramic fuel cells. Nat Energy 2018;3:202–10. doi:10.1038/s41560-017-0085-9.

[9] Wang R, Byrne C, Tucker MC. Assessment of Co-Sintering as a Fabrication Approach for Metal-Supported Proton-Conducting Solid Oxide Cells. Solid State Ionics n.d.

[10] Tucker MC, Ying AS. Metal-supported solid oxide fuel cells operated in direct-flame configuration. Int J Hydrogen Energy 2017;42:24426–34. doi:10.1016/j.ijhydene.2017.07.224.

[11] Tucker MC. Dynamic-temperature operation of metal-supported solid oxide fuel cells. J Power Sources 2018;395:314–7. doi:10.1016/j.jpowsour.2018.05.094.

[12] Tucker MC. Personal power using metal-supported solid oxide fuel cells operated in a camping stove flame. Int J Hydrogen Energy 2018;43:8991–8. doi:10.1016/j.ijhydene.2018.03.161.

[13] Tucker MC. Durability of symmetric-structured metal-supported solid oxide fuel cells. J Power Sources 2017;369:6–12. doi:10.1016/j.jpowsour.2017.09.075.

[14] Leah R, Bone A, Hammer E, Selcuk A, Rahman M, Clare A, et al. Development Progress on the Ceres Power Steel Cell Technology Platform: Further Progress Towards Commercialization. ECS Trans 2017;78:87–95. doi:10.1149/07801.0087ecst.

[15] Tucker MC, Carreon B, Charyasatit J, Langston K, Taylor C, Manjarrez J, et al. Playing with Fire: Commercialization of a Metal-Supported SOFC Product for Use in Charcoal Cookstoves for the Developing World. ECS Trans 2017;78:229–36. doi:10.1149/07801.0229ecst.

[16] Tucker MC. Development of High Power Density Metal-Supported Solid Oxide Fuel Cells. Energy Technol 2017;5:2175–81.

[17] Udomsilp D, Roehrens D, Menzler NH, Bischof C, de Haart LGJ, Opitz AK, et al. High-Performance Metal-Supported Solid Oxide Fuel Cells by Advanced Cathode Processing. J Electrochem Soc 2017;164:F1375–84. doi:10.1149/2.0571713jes.

[18] Nielsen J, Persson ÅH, Muhl TT, Brodersen K. Towards High Power Density Metal

Supported Solid Oxide Fuel Cell for Mobile Applications. J Electrochem Soc 2018;165:F90–6. doi:10.1149/2.0741802jes.

[19] Schiller G, Ansar A, Lang M, Patz O. High temperature water electrolysis using metal supported solid oxide electrolyser cells (SOEC). J Appl Electrochem 2009;39:293–301. doi:10.1007/s10800-008-9672-6.

[20] Chen T, Zhou Y, Liu M, Yuan C, Ye X, Zhan Z, et al. High performance solid oxide electrolysis cell with impregnated electrodes. Electrochem Commun 2015;54:23–7. doi:10.1016/j.elecom.2015.02.015.

[21] Wang R, Dogdibegovic E, Lau GY, Tucker MC. Metal-Supported Solid Oxide Electrolysis Cell (MS-SOEC) With Significantly Enhanced Catalysis. Adv Energy Mater n.d.

[22] Tucker MC. Progress in metal-supported solid oxide fuel cells: A review. J Power Sources 2010;195:4570–82. doi:10.1016/j.jpowsour.2010.02.035.

[23] Larring Y, Fontaine M-L. Critical Issues of Metal-Supported Fuel Cell. Green Energy Technol 2013;55. doi:10.1007/978-1-4471-4456-4.

[24] Krishnan VV. Recent developments in metal-supported solid oxide fuel cells. Wiley Interdiscip Rev Energy Environ 2017:e246. doi:10.1002/wene.246.

[25] Stefan E, Stange M, Denonville C, Larring Y, Hildenbrand N, Norby T, et al. Layered microstructures based on BaZr0.85Y0.15O3−δby pulsed laser deposition for metal-supported proton ceramic electrolyser cells. J Mater Sci 2017;52:6486–97. doi:10.1007/s10853-017-0884-1.

[26] Stange M, Stefan E, Denonville C, Larring Y, Rørvik PM, Haugsrud R. Development of novel metal-supported proton ceramic electrolyser cell with thin film BZY15–Ni electrode

and BZY15 electrolyte. Int J Hydrogen Energy 2017;42:13454–62. doi:10.1016/j.ijhydene.2017.03.028.

[27] Myles TD, Ouimet R, Kwak D, Maric R. Characterization and performance of proton conducting solid oxide fuel cells manufactured using reactive spray deposition technology. ECS Trans 2016;72:17–23. doi:10.1149/07225.0017ecst.

[28] An Intermediate Temperature Metal-Supported Proton-Conducting Solid Oxide Fuel Cell Stack. 18th Annu. SOFC Work., 2017.

[29] Mercadelli E, Gondolini A, Pinasco P, Sanson A, Barison S, Fabrizio M. Key Issues in Processing Metal-Supported Proton Conducting Anodes for SOFCs Applications. ECS Trans 2011;35:1761–9. doi:10.1149/1.3570164.

[30] Dogdibegovic E, Wang R, Lau GY, Tucker MC. High performance metal-supported solid oxide fuel cells with infiltrated electrodes. J Power Sources 2019;410–411:91–8.

[31] Tucker MC, Lau GY, Jacobson CP, DeJonghe LC, Visco SJ. Performance of metal-supported SOFCs with infiltrated electrodes. J Power Sources 2007;171:477–82. doi:10.1016/j.jpowsour.2007.06.076.

[32] Dayaghi AM, Kim KJ, Kim SJ, Park J, Kim SJ, Park BH, et al. Stainless steel-supported solid oxide fuel cell with La0.2Sr0.8Ti0.9Ni0.1O3−δ/yttria-stabilized zirconia composite anode. J Power Sources 2016;324:288–93. doi:10.1016/j.jpowsour.2016.05.076.

[33] Sawant P, Varma S, Wani BN, Bharadwaj SR. Synthesis, stability and conductivity of BaCe0.8-xZrxY0.2O3-δas electrolyte for proton conducting SOFC. Int J Hydrogen Energy 2012;37:3848–56. doi:10.1016/j.ijhydene.2011.04.106.

[34] Liu M, Liu Y, Yang L, Liu M, Tang Z. Enhanced sinterability of BaZr0.1Ce0.7Y0.1Yb0.1O3-δby addition of nickel oxide. J Power Sources

2011;196:9980–4. doi:10.1016/j.jpowsour.2011.08.047.

[35] Babilo P, Uda T, Haile SM. Processing of yttrium-doped barium zirconate for high proton conductivity. J Mater Res 2007;22:1322–30. doi:10.1557/jmr.2007.0163.

[36] Yamazaki Y, Hernandez-Sanchez R, Haile SM. Cation non-stoichiometry in yttrium-doped barium zirconate: Phase behavior, microstructure, and proton conductivity. J Mater Chem 2010;20:8158–66. doi:10.1039/c0jm02013c.

[37] Cheng L, Park JS, Hou H, Zorba V, Chen G, Richardson T, et al. Effect of microstructure and surface impurity segregation on the electrical and electrochemical properties of dense Al-substituted Li7La3Zr2O12. J Mater Chem A 2014;2:172–81. doi:10.1039/c3ta13999a.

[38] Shima D, Haile SM. The influence of cation non-stoichiometry on the properties of undoped and gadolinia-doped barium cerate. Solid State Ionics 1997;97:443–55. doi:10.1016/S0167-2738(97)00029-5.

[39] Hou Y, Wu J, Konysheva EY. Quantitative characterization of Cr-adsorption on CeO2, pure and doped BaCeO3 and its impact on the electrochemical performance of Ce containing complex oxides. Int J Hydrogen Energy 2016;41:3994–4004. doi:10.1016/j.ijhydene.2015.12.168.

[40] Zhao L, Ding D, Zhang L, Gui L, Wang Z, Wan Y, et al. The effect of Cr deposition and poisoning on BaZr0.1Ce0.7Y0.2O3-δproton conducting electrolyte. Int J Hydrogen Energy 2014;39:18379–84. doi:10.1016/j.ijhydene.2014.09.009.

[41] Kammer Hansen K, Menon M, Knudsen J, Bonanos N, Mogensen M. The Effect of a CGO Barrier Layer on the Performance of LSM/YSZ SOFC Cathodes. J Electrochem Soc 2010;157:B309. doi:10.1149/1.3273194.

[42] Montaleone D, Mercadelli E, Gondolini A, Pinasco P, Sanson A. On the compatibility of

dual phase BaCe0.65Zr0.2Y0.15O3-based membrane for hydrogen separation application. Ceram Int 2017;43:10151–7. doi:10.1016/j.ceramint.2017.05.039.

[43] Babilo P, Haile SM. Enhanced sintering of yttrium-doped barium zirconate by addition of ZnO. J Am Ceram Soc 2005;88:2362–8. doi:10.1111/j.1551-2916.2005.00449.x.

[44] Tsai CL, Kopczyk M, Smith RJ, Schmidt VH. Low temperature sintering of Ba(Zr0.8 - XCexY0.2)O3 - δusing lithium fluoride additive. Solid State Ionics 2010;181:1083–90. doi:10.1016/j.ssi.2010.06.028.

[45] Li Y, Guo R, Wang C, Liu Y, Shao Z, An J, et al. Stable and easily sintered BaCe0.5Zr0.3Y0.2O3-δelectrolytes using ZnO and Na2CO3additives for protonic oxide fuel cells. Electrochim Acta 2013;95:95–101. doi:10.1016/j.electacta.2013.02.023.

[46] Nikodemski S, Tong J, O'Hayre R. Solid-state reactive sintering mechanism for proton conducting ceramics. Solid State Ionics 2013;253:201–10. doi:10.1016/j.ssi.2013.09.025.